This is the accepted manuscript made available via CHORUS. The article has been published as:

# Highly ordered nanoscale patterns produced by masked ion bombardment of a moving solid surface

Martin P. Gelfand and R. Mark Bradley

Phys. Rev. B **86**, 121406 — Published 21 September 2012

DOI: 10.1103/PhysRevB.86.121406

# Highly-Ordered Nanoscale Patterns Produced by Masked Ion Bombardment of a Moving Solid Surface

Martin P. Gelfand* and R. Mark Bradley†
*Department of Physics, Colorado State University, Fort Collins, Colorado 80523*
(Dated: September 11, 2012)

We introduce a fabrication method in which a mask with a long, narrow slit is placed between the source of an ion beam and the surface of a solid moving with constant speed. Numerical simulations reveal the method can generate surface ripples and arrays of nanoholes that are virtually defect-free. In contrast, the patterns produced by ion bombardment with a broad, unmasked beam are typically rife with defects.

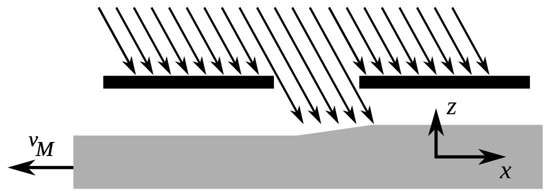


FIG. 1. Schematic illustration of a moving sample undergoing masked ion bombardment. The "active region" of the sample surface is subject to bombardment; the "eroded region" is to the left of the active region and the "uneroded region" is to the right.

Bombarding a nominally flat solid surface with a broad ion beam can produce an impressive variety of self-assembled patterns with feature sizes as small as 10 nm. These patterns include periodic height modulations or "ripples" produced by oblique-incidence ion bombardment (OIIB),[1] as well as hexagonal arrays of nanodots or nanoholes that are generated by normal-incidence bombardment.[2–7] The spontaneous emergence of these patterns is not just fascinating in its own right: ion bombardment has the potential to become a cost-effective method to rapidly fabricate large-area nanostructures at length scales beyond the limits of conventional optical lithography.

A serious issue that has diminished the utility of ion-induced pattern formation is the presence of numerous defects in the patterns that are usually produced. When an entire nominally flat sample surface is subjected to OIIB, the ripples that begin to develop on different regions of the surface are out of phase, and defects form where these ordered patches meet. Limited progress has been made in reducing the number of defects in surface ripples—for example, experiments have shown that few defects form near the boundary of a region subjected to OIIB.[8] Similarly, if the surface is pre-patterned with parallel trenches with a width equal to a few times the ripple wavelength, the ripples that form in the trenches tend to align with the trench walls, and the number of defects in the ripple patterns is small.[9] Both of these methods only suppress defects in the immediate vicinity of the boundary or wall. Perfectly ordered ripples could of course be produced by simply rastering a tightly focused ion beam over the surface with sufficient separation between adjacent lines, and hexagonally ordered nanohole arrays could be fabricated by direct ion beam writing as well. Ion beam writing is time-consuming, inefficient and expensive, however.

In this Rapid Communication, we carry out a theoretical study of a fabrication method in which a middle ground is struck between the extremes of using a broad, unfocused beam and a tightly focused and controlled beam. Our simulations reveal that a rich variety of patterns can form, including highly-ordered ripples and (to our complete surprise) arrays of nanoholes of astonishing regularity. The proposed method may therefore provide a generally applicable means of surmounting a key obstacle that has prevented the widespread adoption of ion bombardment as a nanoscale fabrication tool—the high density of defects in the patterns that are normally produced.

Consider a solid whose surface would occupy the $x-y$ plane if it were not slightly rough. In our fabrication method, a mask is employed to produce an ion beam that is confined to the region $0 \le x \le L$, and the sample is translated at constant speed $v_M$ in the $-x$ direction: see Fig. 1. The mask could be composed of the same material as the sample to avoid the introduction of impurities. Alternatively, one could employ a focused ion beam which has been defocused along the $y$-direction, or sweep a focused beam rapidly back and forth along the $y$-direction. The direction of the incident ions is chosen so that if the mask were not present, surface ripples would form with their wave vector along the $x$ axis. This means that the angle of incidence $\theta$ must lie between two critical values $\theta_1$ and $\theta_2$ that depend on the target material as well as the ion species and energy.

At first glance, it would seem that this procedure would force the ripples to have the same phase all along the leading edge of the bombarded region, the line $x = L$. We might therefore anticipate that ripples with a reduced density of defects would be produced, or perhaps even perfectly ordered ripples. This idea is given additional support by the experimental results of Ichim and Aziz.[8] Although we do find that highly regular ripples form for certain ranges of parameters, other types of patterns also emerge.

To begin our analysis, consider a nearly planar surface of an elemental solid that is subjected to unmasked OIIB. We assume that the solid is amorphous, or that a surface layer of the solid is rendered amorphous by the bombardment. Including the lowest order nonlinear terms,[10,11] the equation of motion in the frame of reference of the sample is the two-dimensional, anisotropic Kuramoto-Sivashinsky (KS) equation for the surface height $h(x, y, t)$,

$$h_t = -v_0 - v_1 h_x - h_{xx} - \alpha h_{yy} - \tfrac{1}{2} h_x^2 - \tfrac{1}{2}\beta h_y^2 - \nabla^2\nabla^2 h, \qquad (1)$$

where $v_0$, $v_1$, $\alpha$, and $\beta$ are constants and the subscripts $x$, $y$, and $t$ denote partial derivatives. We have chosen units for time and the three spatial coordinates so as to make the coefficients of $h_{xx}$, $h_x^2$, and $\nabla^2\nabla^2 h$ assume the given form.

The constant term on the right-hand side of Eq. (1) is the erosion velocity of a planar surface, while the second term stems from the dependence of the sputter yield on the local angle of incidence. The terms proportional to $h_{xx}$ and $h_{yy}$ describe the effects of the curvature dependence of the sputter yield[12] and the Carter-Vishnyakov effect.[13–18] If the angle of incidence $\theta$ is equal to $\theta_1$, the parameter $\alpha = -\infty$. The value of $\alpha$ is an increasing function of $\theta$ that exceeds unity once $\theta$ has exceeded the second critical angle $\theta_2$. Because we have assumed that $\theta_1 < \theta < \theta_2$, we must have $\alpha < 1$. Depending on the nature of the target material, the physical origin of the final term on the right-hand-side of Eq. (1) is either surface diffusion or ion-induced viscous flow within a thin layer at the solid surface.[19] If the source of this term is surface diffusion, we take the sample temperature to be low enough that thermally-activated diffusion is negligible, so that the diffusion is ion-induced.

Now suppose that a mask that has a narrow slit running parallel to the $y$-axis is interposed between the ion source and the sample surface. In the rest frame of the sample, the mask moves in the $+x$ direction with constant speed $v_M$ and its left edge is at the position $x_M(t) = v_M t$. We will describe the $x$-dependence of the ion flux by a non-negative "mask function" $M(x,t)$ that is nonzero only on the interval $x_M(t) < x < x_M(t) + L$, the "active region". $M$ has a maximum value of 1; this value is the normalized flux in the absence of the mask. The portion of the sample with $x < x_M(t)$, the eroded region, does not evolve further, while the uneroded region is taken to have a narrow, uncorrelated Gaussian height distribution meant to model low-amplitude roughness of the pristine surface. The coefficients of all the terms on the right-hand side of Eq. (1) except the last are manifestly proportional to the ion flux. Because we have assumed that ion bombardment is the source of the last term, the surface mobility is linear in the ion flux and $\nabla^2\nabla^2 h$ is replaced by $\nabla \cdot [M(x,t)\nabla(\nabla^2 h)]$. Transforming to a frame co-moving with the mask leads to the equation that we will solve numerically,

$$\begin{aligned} h_t = {} & [v_M - v_1 M(x)]h_x \\ & + M(x)\left(-v_0 - h_{xx} - \alpha h_{yy} - \tfrac{1}{2}h_x^2 - \tfrac{1}{2}\beta h_y^2\right) \\ & - \nabla \cdot \left[M(x)\nabla(\nabla^2 h)\right] \, . \end{aligned} \tag{2}$$

In this frame the mask function $M(x) \equiv M(x, t = 0)$ is time-independent.

If the surface height $h$ is independent of the transverse coordinate $y$, our model becomes one-dimensional (1D), and it then resembles a model of waterjet cutting introduced by Friedrich *et al.*[20] The key result obtained by Friedrich *et al.* was that the eroded region changes from being flat to being rippled as $v_M$ is reduced. We have also explored 1D models, but primarily considered the effect of varying the width of the active region $L$ rather than the speed $v_M$. There is, as one would anticipate, a transition between a flat and a rippled surface if the width is increased while the other parameters are held fixed.

Our numerical integrations of Eq. (2) are based on lowest-order, centered finite-difference approximations for all of the spatial derivatives except for the advective term. For the advective term we use linear upwind differencing in the active region, and in the eroded region the advection is treated exactly. A square spatial grid with side length $\Delta x$ is employed in the active region; for time evolution there we use the Crank-Nicholson scheme for the linear terms and the explicit Euler scheme for the nonlinear and mean erosion ($v_0$) terms, following Rost and Krug.[21] For nearly all calculations we took $\Delta x = 0.25$ (which is to be compared with $\lambda_{\text{lin}} = 2\sqrt{2}\pi \approx 8.89$, the most unstable wavelength of the unmasked linear problem) and $\Delta t = 0.001$.

We impose periodic boundary conditions in the $y$ direction and denote the number of grid points along the $y$ axis by $N_y$. For the mask function we adopted a trapezoidal form

$$M(x) = \begin{cases} x/B & x \in [0, B] \\ 1 & x \in [B, B+W] \\ 1 - (x - W - B)/B & x \in [B+W, 2B+W], \end{cases} \tag{3}$$

where $2B + W = L$. Since $M$ appears under a derivative in the final term of Eq. (2), we chose a continuous mask function, rather than the truncated Gaussian employed by Friedrich *et al.* (whose equation of motion had the final term $-M(x)\nabla^2\nabla^2 h$ rather than $-\nabla \cdot \left[M(x)\nabla(\nabla^2 h)\right]$). By using a different mask function than Friedrich *et al.* we also demonstrate that in 1D the existence of a transition between flat and periodic surface profiles is independent of the detailed form of the mask and the term that involves four spatial derivatives.

Because our model has seven parameters ($v_0$, $v_1$, $\alpha$, $\beta$, $v_M$, $W$, and $B$), constructing a complete phase diagram of the steady-state structures it produces would be impractical. Instead, we have identified some of the typical patterns formed by the model. It is helpful to begin by considering the 1D version, which removes two parameters, $\alpha$ and $\beta$, and can be simulated much more quickly than the 2D model. After some initial exploration of the effects of varying the parameters, we restricted our attention to the representative parameter values $v_0 = 1/40$, $v_1 = 0$, $v_M = 1$, and $B = 4$. We find a transition from a flat to a rippled steady-state structure at $W \equiv W_1 \approx 3.89$, with a wavelength slightly longer than $\lambda_{\text{lin}}$ in the rippled state. Increasing $W$ still further only leads to small changes in the wavelength of the ripples until $W = W_2 \approx 6.4$, where a "period-doubled" state develops. Figure 2 shows examples of the three states

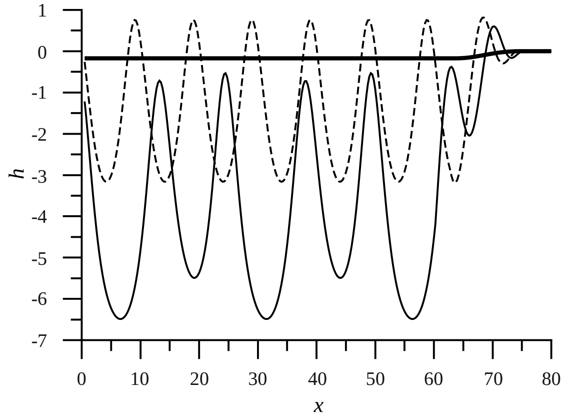


FIG. 2. Steady-state results for the 1D model with $W = 3$ (thick solid line), $W = 4$ (dashed line), and $W = 6.5$ (thin solid line). The origin has been adjusted in each case so that $x = 75$ corresponds to the leading edge of the active region.

just described. For large enough $W$ a chaotic state emerges. There are in fact hints of a complete period-doubling route to chaos, which is akin to the behavior of the 1D KS equation with periodic boundary conditions as the ratio of the domain width to $\lambda_{\text{lin}}$ is varied.[22]

Now consider the 2D model. Are the 1D structures stable? In our simulations we typically took $N_y = 300$, i.e., a strip of width 75, but increased $N_y$ to 500 when we suspected $N_y$-dependent artifacts.[23] We will only describe results with $\beta = 1$, since we have found little dependence on that parameter.[24] The parameter $\alpha$ is much more interesting: in the absence of the mask $\alpha > 0$ corresponds to linear instability of the uniform state with respect to sufficiently long wavelength perturbations along the $y$ direction while $\alpha < 0$ corresponds to stability, and so one might anticipate very different behaviors depending on the sign of $\alpha$. The actual behavior is more complicated.

For $W \lesssim W_1$, we find that the flat state is stable, even when $\alpha$ is as large as 0.4. Remarkably, the transverse instability that would occur for positive $\alpha$ if no mask were present is suppressed by a mask that only restricts the ion flux in the $x$ direction. We speculate that this instability has insufficient time to develop before the active region has moved on to the adjacent portion of the target surface.

Fig. 3(a) shows the results of a simulation with $W = 4 > W_1$ and $\alpha = 0.05$. After a transient, completely defect-free ripples develop. The entire sample was in fact much longer along the $x$ direction than shown in the figure, but there was no change from the behavior at the largest $x$ that is shown. Note that close to the flat/rippled transition, the rippled state is stable in 2D even when $\alpha > 0$, provided that $\alpha$ is not too large.

For somewhat greater $W$ values, something unexpected transpires: the rippled state becomes unstable with respect to perturbations along the $y$ direction and evolves into an amazingly well ordered, nearly hexagonal array of nanoholes. Fig. 3(b) shows the results of a simulation with $W = 6$ and $\alpha = 0$. The evolution with increasing $x$ shows first a rippled structure developing and saturating by $x \approx 200$. By $x \approx 350$ the instability along the $y$ direction can be seen in the figure, and by $x \approx 600$ that secondary instability has saturated.

The emergence of a well ordered nanohole array is not limited to the marginal case of $\alpha = 0$: it is seen for positive $\alpha$ and, provided that $\alpha$ is not too large in magnitude and $W$ is big enough, for *negative* $\alpha$ as well. This is surprising, given that the in the absence of the mask, the solid surface is stable with respect to perturbations along the $y$-direction for $\alpha < 0$. Our simulations suggest that the time needed for the secondary instability to set in is a decreasing function of $\alpha$, and that sufficiently negative $\alpha$ completely suppresses it.

Another modest increase in $W$, to 7 (and with $\alpha = 0$, not that its value is critical here), leads to a transient quasi-one-dimensional chaotic pattern and then to a fully 2D chaotic state, as shown in Fig. 3(c). Finally, Fig. 3(d) shows a case between the latter two, with $W = 6.5$ and $\alpha = 0$, that illustrates the robustness of the nanohole array state. As was seen in Fig. 2, the 1D model with this value of $W$ exhibits period-doubled ripples; they can be seen in Fig. 3(d) shortly after the amplitude has saturated, for $200 \lesssim x \lesssim 300$. The secondary instability then develops and there is a lengthy interval in which defects heal, but by $x = 1100$ the ordered 2D pattern is established.

The results of several dozen simulations are summarized in the $W$-$\alpha$ phase diagram shown in Fig. 4. The phase boundaries are meant only to be guides to the eye, and have not been joined since we do not have sufficient information to determine the topology of the phase diagram. It is clear that rippled structures occupy a significant portion of the phase diagram, especially for $\alpha < 0$; and that nanohole arrays, though occupying a nontrivial area of the phase diagram, require more careful tuning of the parameters.

Arrays of nanodots[2,6,7] and nanoholes[5] with a degree of hexagonal order have been produced by bombardment with

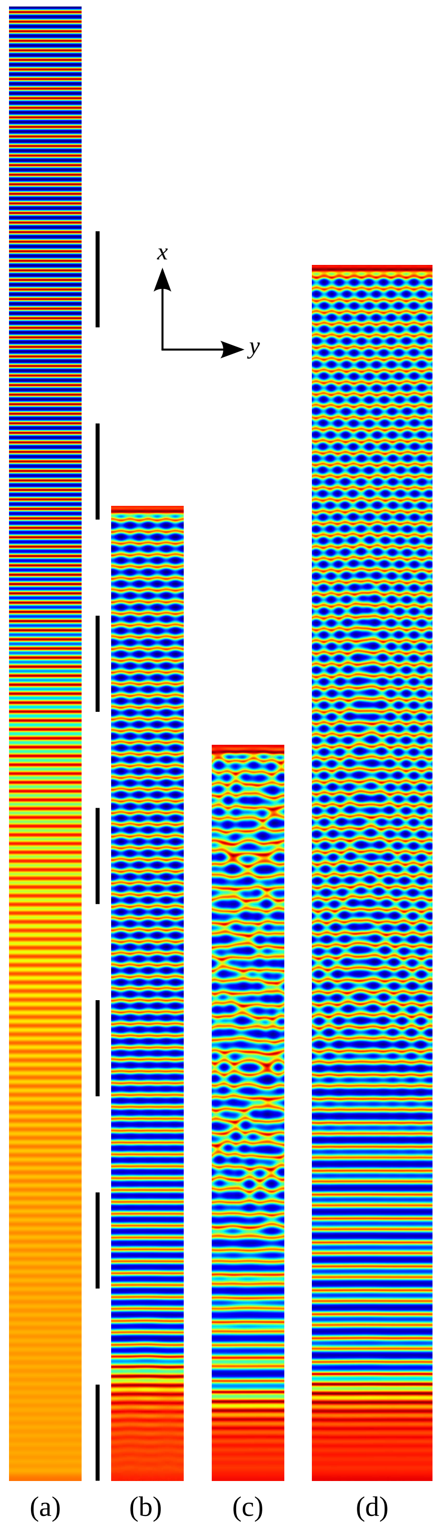


FIG. 3. (Color online) Simulations with parameters described in the text. Red corresponds to the largest values of $h$ in each dataset while blue corresponds to the smallest. The same scale is used for the in-plane coordinates in each part, and the scale is the same for the $x$ and $y$ directions. The vertical black lines have length 100, as do the gaps between them. In (b), (c) and (d) the eroded and active regions are displayed; while in (a) the figure is cut off well before the active region.

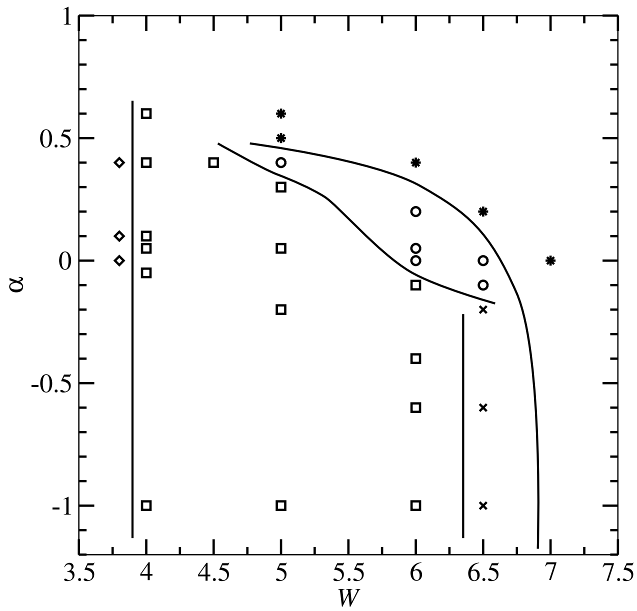


FIG. 4. Schematic phase diagram in the $W$-$\alpha$ plane, with other parameters taking the values $v_0 = 1/40$, $v_1 = 0$, $v_M = 1$, $B = 4$, and $\beta = 1$. Each symbol represents a simulation, with the structures exhibited at long time indicated by $\diamondsuit$ for flat, $\square$ for ripples, $\times$ for period-doubled ripples, $\circ$ for quasi-hexagonal arrays of holes, and $*$ for chaotic. The lines separating the phases are just guides to the eye. The structures seen at $\alpha = -1$ agree with those in the 1D calculations, corresponding to $\alpha = -\infty$, and so the true phase boundaries are likely to be nearly vertical for sufficiently negative $\alpha$. Note also that there are additional structures not shown on this diagram, such as period-quadrupled ripples.

a broad ion beam, but only for a few select choices of target material and ion species.[2,5–7] Our method, by contrast, could in principle be used to produce highly ordered nanohole arrays on any elemental material.

Very recently, Motta *et al.* have shown that OIIB of a binary material with a broad ion beam can produce very regular surface ripples if the angle of incidence, ion energy and ion species are appropriately chosen.[25] This high degree of order is a result of the coupling between the surface height and composition of the binary material, and so cannot be achieved by bombarding an elemental material with a broad ion beam. The fabrication method proposed in this paper has the advantage that it could be applied to generate highly ordered ripples on the surface of an elemental material.

The price that must be paid for the dramatically improved order and the flexibility in choice of target offered by our proposed method, compared to methods based on broad-beam bombardment, is greatly reduced processing speed—since only a small portion of the surface is subject to bombardment at a given time. However, one could conceive of a mask composed of many identical, parallel slits. Whether such a mask could produce well ordered ripples or nanoholes over an entire surface, while sacrificing far less processing speed than a single-slit mask, is an interesting question for future study.

In summary, in this Letter we introduced a fabrication method in which a mask is used to produce an ion beam that is confined to the region $0 \leq x \leq L$, and the target is translated at constant speed in the $-x$ direction. Simulations indicate that the method can yield remarkably defect-free nanoscale surface ripples and arrays of holes. We expect that even more interesting types of pattern formation will emerge if the target is a binary material, and plan to address that topic in future work.

## ACKNOWLEDGMENTS

This research of M.P.G. was supported by the National Science Foundation under Grant No. CHE-1059089.

* martin.gelfand@colostate.edu
† bradley@lamar.colostate.edu

[1] See, for example, J. Muñoz-García, L. Vázquez, R. Cuerno, J. A. Sánchez-García, M. Castro, and R. Gago, in *Toward Functional Nanomaterials*, Lecture Notes in Nanoscale Science and Technology, Vol. 5 (Springer, 2009) pp. 323–398.
[2] S. Facsko, T. Dekorsy, C. Koerdt, C. Trappe, H. Kurz, A. Vogt, and H. L. Hartnagel, Science **285**, 1551 (1999).
[3] R. M. Bradley and P. D. Shipman, Phys. Rev. Lett. **105**, 145501 (2010).
[4] P. D. Shipman and R. M. Bradley, Phys. Rev. B **84**, 085420 (2011).
[5] Q. Wei, X. Zhou, B. Joshi, Y. Chen, K.-D. Li, Q. Wei, K. Sun, and L. Wang, Adv. Mater. **21**, 2865 (2009).
[6] L. Bischoff, W. Pilz, and B. Schmidt, Applied Physics A: Materials Science & Processing **104**, 1153 (2011).
[7] L. Bischoff, K.-H. Heinig, B. Schmidt, S. Facsko, and W. Pilz, Nucl. Instrum. Methods Sect. B **272**, 198 (2012).
[8] S. Ichim and M. J. Aziz, J. Vac. Sci. Technol. B **23**, 1068 (2005).
[9] A. Cuenat, H. B. George, K.-C. Chang, J. M. Blakely, and M. J. Aziz, Adv. Mater. **17**, 2845 (2005).
[10] R. Cuerno and A.-L. Barabási, Phys. Rev. Lett. **74**, 4746 (1995).
[11] M. A. Makeev, R. Cuerno, and A.-L. Barabási, Nucl. Instrum. Methods Sect. B **197** (2002).
[12] R. M. Bradley and J. M. E. Harper, J. Vac. Sci. Technol. A **6**, 2390 (1988).
[13] G. Carter and V. Vishnyakov, Phys. Rev. B **54**, 17647 (1996).
[14] M. Moseler, P. Gumbsch, C. Casiraghi, A. C. Ferrari, and J. Robertson, Science **309**, 1545 (2005).
[15] B. Davidovitch, M. J. Aziz, and M. P. Brenner, Phys. Rev. B **76**, 205420 (2007).
[16] C. S. Madi, E. Anzenberg, K. F. Ludwig, and M. J. Aziz, Phys. Rev. Lett. **106**, 066101 (2011).
[17] S. A. Norris, J. Samela, L. Bukonte, M. Backman, F. Djurabekova, K. Nordlund, C. S. Madi, M. P. Brenner, and M. J. Aziz, Nature Comm. **2**, 276 (2011).
[18] M. Castro and R. Cuerno, Applied Surface Science **258**, 4171 (2012).
[19] C. C. Umbach, R. L. Headrick, and K.-C. Chang, Phys. Rev. Lett. **87**, 246104 (2001).
[20] R. Friedrich, G. Radons, T. Ditzinger, and A. Henning, Phys. Rev. Lett. **85**, 4884 (2000).
[21] M. Rost and J. Krug, Phys. Rev. Lett. **75**, 3894 (1995).
[22] Y. S. Smyrlis and D. T. Papageorgiou, Proc. Natl. Acad. Sci. USA **88**, 11129 (1991).
[23] For example, if we observed a pattern with anomalously long wavelength along the $y$ direction, we changed the width of the sample to determine whether that was due to incommensurability between the natural wavelength in the $y$ direction and the sample width.
[24] We have only considered positive values of $\beta$. For negative values of this parameter, so-called "cancellation modes" occur.[21] These have not been observed in experiments and their appearance would necessitate the retention of higher order nonlinear terms in the equation of motion.
[25] F. C. Motta, P. D. Shipman, and R. M. Bradley, J. Phys. D **45**, 122001 (2012).